JACS
JOURNAL OF THE AMERICAN CHEMICAL SOCIETY
pubs.acs.org/JACS
Article

Structural Disorder as the Origin of Optical Properties and Spectral Dynamics in Squaraine Nano-Aggregates

Robin Bernhardt,* Marìck Manrho, Jennifer Zablocki, Lukas Rieland, Arne Lützen, Manuela Schiek, Klaus Meerholz, Jingyi Zhu,* Thomas L. C. Jansen, Jasper Knoester, and Paul H. M. van Loosdrecht*

Cite This: J. Am. Chem. Soc. 2022, 144, 19372−19381
Read Online
ACCESS | Metrics & More | Article Recommendations | Supporting Information

ABSTRACT: In contrast to regular J- and H-aggregates, thin film squaraine aggregates usually have broad absorption spectra containing both J-and H-like features, which are favorable for organic photovoltaics. Despite being successfully applied in organic photovoltaics for years, a clear interpretation of these optical properties by relating them to specific excited states and an underlying aggregate structure has not been made. In this work, by static and transient absorption spectroscopy on aggregated *n*-butyl anilino squaraines, we provide evidence that both the red- and blue-shifted peaks can be explained by assuming an ensemble of aggregates with intermolecular dipole−dipole resonance interactions and structural disorder deriving from the four different nearest neighbor alignments—in sharp contrast to previous association of the peaks with intermolecular charge-transfer interactions. In our model, the next-nearest neighbor dipole−dipole interactions may be negative or positive, which leads to the occurrence of J- and H-like features in the absorption spectrum. Upon femtosecond pulse excitation of the aggregated sample, a transient absorption spectrum deviating from the absorbance spectrum emerges. The deviation finds its origin in the excitation of two-exciton states by the probe pulse. The lifetime of the exciton is confirmed by the band integral dynamics, featuring a single-exponential decay with a lifetime of 205 ps. Our results disclose the aggregated structure and the origin of red- and blue-shifted peaks and explain the absence of photoluminescence in squaraine thin films. Our findings underline the important role of structural disorder of molecular aggregates for photovoltaic applications.

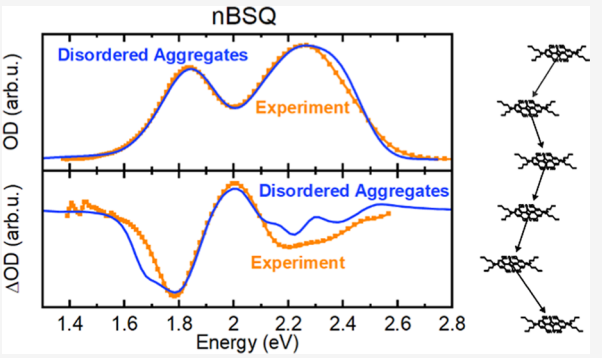

INTRODUCTION

Aggregated molecular assemblies have attracted considerable interest in many fields of scientific research and technological development,[1−6] especially for organic optoelectronic devices[7−10] such as light emitting diodes and solar cells. Their optoelectronic properties depend strongly on the aggregates' structure and morphology, making an understanding of these properties essential to understanding and tuning device performance. In aggregates of molecules with strong optical transitions, the resonance Coulomb interactions between the associated transition dipole moments can yield large spectral shifts, cause changes in absorption linewidths, as well as enhance or quench fluorescent emission. Based on these dipolar interactions of transition dipole moments, two archetypes of aggregates named J- and H-aggregates[11−13] can be formed depending on the relative alignment of the transition dipole moments. In the special case of parallelly aligned transition dipole moments, the slip angle θ between them and the relative position vector connecting two molecules dictates the interaction between them. Importantly, this interaction may either be positive, for $\theta > 54.7°$, or negative, for $\theta < 54.7°$.[12,14] This provides a general picture for understanding the spectroscopic properties of molecular aggregates with parallel transition dipoles. Depending on the slip angle, they may either exhibit a bright state at the high-energy side of the exciton band and a dark state at its low-energy side, as is the case for H-aggregates, or vice versa for J-aggregates.

Although the simple model of J- and H-type aggregates explains the basic spectral properties of many molecular aggregates, there are also many aggregates for which the simple J- and H-picture does not hold and that require a more complicated model.[15] Even for a simple dimer structure, the resonance interaction between chromophores with non-parallel transition dipole moments[16,17] and charge-transfer interactions[18,19] may split the exciton band. Also, the aggregate morphology is important: for aggregates with a tubular

Received: July 5, 2022
Published: October 14, 2022

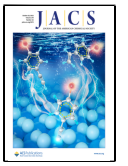

https://doi.org/10.1021/jacs.2c07064
J. Am. Chem. Soc. 2022, 144, 19372−19381

symmetry, multiple J-bands may occur or even multiple J- and H-bands.[20,21] Similarly, structural disorder and inhomogeneity of the environment can significantly broaden the spectroscopic response of molecular aggregates. Molecular vibrations further enrich the optical properties. Models including vibrations have been developed based on either dimer-[22−24] or crystal-like aggregation[25,26] and have been successfully applied to aggregated systems such as TDBC—a cyanine dye—and pseudoisocyanine dyes.[27,28] In short, there are abundant effects that may complicate aggregate spectra beyond the simple J- and H-band picture. Thus, detailed knowledge of packing, morphology, and additional interactions may be needed for modeling aggregate spectra and optical dynamics.

An unusual aggregation system deviating significantly from the basic J- and H-picture is found for certain squaraine dyes. Due to their unique and easily customizable optical properties[29,30] this large family of π-conjugated quadrupolar molecules has attracted attention in recent experimental[17,31−38] and theoretical studies.[39−44] As reported, the molecules can easily form either J- or H-type aggregates depending on their molecular structure[32,33,36] and sample preparation conditions.[34,35,45,46] Moreover, squaraines with a symmetric molecular backbone show strong electron-donating and -accepting properties, and both intra- and inter-molecular charge transfer could play an important role in the optical spectra of squaraine aggregates.[47] Recently, a family of *n*-alkyl aniline squaraines (see Figure 1a) was synthesized and

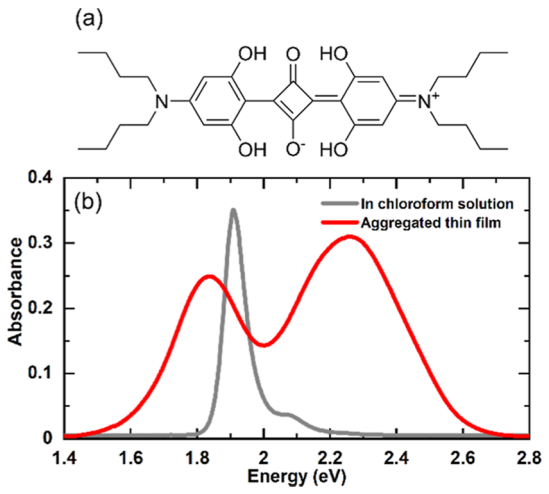

Figure 1. Molecular structure and steady-state absorption of nBSQ samples. (a) Chemical skeleton of the monomer nBSQ in the $x-y$ plane of molecular coordinates. (b) Steady-state absorbance spectra of monomeric nBSQ in chloroform solution (gray line) and aggregated thin films on glass substrates (red line).

engineered[48,49] for organic solar cells which can reach relatively high power conversion efficiencies. The monomeric squaraines contain a strong hydrogen bond network forming a very rigid planar skeleton and can be referred to as a donor−acceptor−donor system (D−A−D). When forming aggregated solid films, both "J-" and "H-like" transitions were observed simultaneously, while the samples lacked any photoluminescence (see Figures 1b, S2 and ref 49). Note that the terms "J-/H-like" are used for simplicity to assign the features in the absorption spectrum that are red- and blue-shifted relative to the monomer absorption peak.

Surprisingly, despite many efforts and successes made for solar cell application, little is known about the nature of the electronic states in these aggregates and the mechanisms of their formation and structure. To explain the experimentally observed broad optical transitions and lack of photoluminescence, an intermolecular charge transfer model[47] based on a simple dimer analysis has been proposed. However, until now, no direct experimental evidence of charge separation has been observed, and it is not clear how the aggregated structure is related to the intermolecular charge separation in longer and disordered aggregates. Recently, a similar dimer system was modeled,[50] suggesting that strong quadrupolar interactions can explain a "red-shifted H-aggregate".

Missing aspects of the quest to understand the optical properties of *n*-alkyl anilino squaraines are the effects of aggregate size and structural disorder. As previous studies[47,50] are based on the sophisticated but computationally costly essential states model[51] that includes intermolecular charge transfer, the aggregate size that may be considered in the numerical analysis is very limited. In this study, we will use a much simpler exciton model, in which only dipolar resonance interactions between the molecules are taken into account, a physically plausible form of structural (packing) disorder is considered, and intermolecular charge transfer is ignored. This model is a further simplification with respect to previous studies using the essential states model without charge-transfer interactions.[50,52] This allows us to model long aggregates and to systematically study the effects of structural disorder, enabling us to show that this simple model explains the measured steady state and broadband transient absorption spectra of thin films of the rigid planar molecule 2,4-bis[4-(*N*,*N*-dibutylamino)-2,6-dihydroxyphenyl]-squaraine (nBSQ).

The aggregate excitons decay single exponentially with a lifetime of around 200 ps and show photobleaching and two-exciton absorption in both red- and blue-shifted absorption regions, suggesting a single aggregate system. Not only the steady-state absorption but also the transient response is in good agreement with the proposed model if two-exciton states are properly included. Our results indicate that nBSQ thin films consist of disordered nanoscale aggregates with excitons delocalized over approximately 10 molecules, stimulating new thoughts about the role of structural disorder for engineering optical properties of molecular aggregates.

Structural Model and Theory. The aggregate model proposed here has two main ingredients, namely (i) a specific form of structural disorder and (ii) dipole−dipole resonance (excitation transfer) interactions between the molecules that make up the aggregate. The symmetry of nBSQ molecules (Figure 1a) acts as a starting point to simulate an aggregate's disordered structure. A single molecule contains two *n*-butyl-functionalized anilino rings, which behave as electron donors, and a central squaric acid-derived group, which acts as an electron acceptor. The whole D−A−D-like molecule has a D_{2h} symmetry around the squaric center. The molecule's symmetric charge distribution results in the absence of a permanent electric dipole moment. Furthermore, a strong hydrogen bond network between the phenol hydroxyl groups and the carbonyl oxygen atoms confines the molecule's skeleton into a rigid plane. Thus, both the π-conjugated orbitals and the Coulomb interaction between charge sites steer molecular aggregation. For visualization, the concept is explained using the *x*,*y*,*z*-coordinate system as in Figure 2a,b.

https://doi.org/10.1021/jacs.2c07064
J. Am. Chem. Soc. 2022, 144, 19372−19381

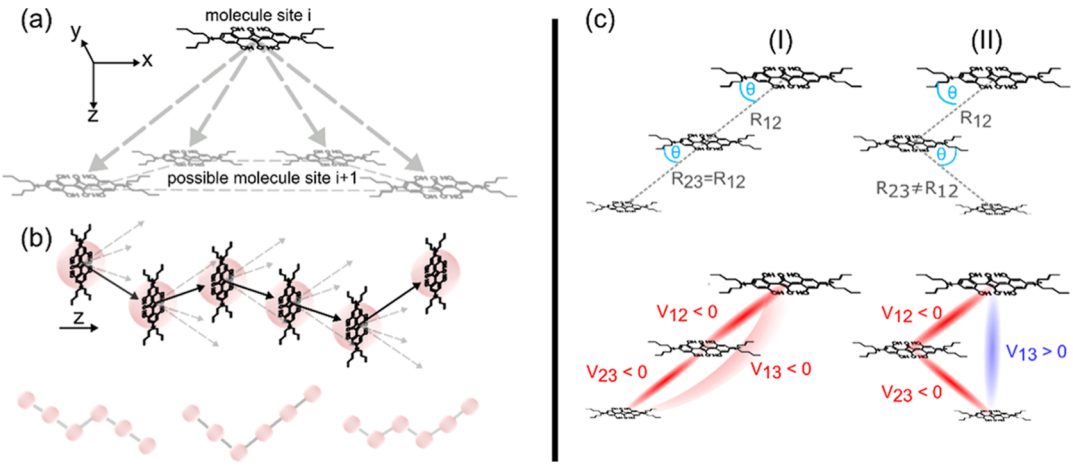

Figure 2. Proposed structural model of nBSQ aggregates. (a) For the sequential construction of an aggregate, a new molecule is allowed to occupy one of four spots relative to the previous molecule. (b) Random sequential construction of aggregates yields a disordered aggregate chain. Every construction yields a different structure. (c) Two types of trimers—straight (I) and kinked (II)—demonstrate the influence of structure on the dipolar interaction between the next-nearest neighbors.

The symmetry of nBSQ and the position of its charges allow us to predict the packing of molecules inside an aggregate. First, neighboring molecules will align their planes parallel to each other. Second, they will be shifted in both the x- and y-direction to optimize their ground-state Coulomb interaction. The resulting translation vector $\vec{R}_{i,i+1}$ between the nearest neighbors can be parameterized as $(\Delta x, \Delta y, \Delta z)$, with Δx, Δy, $\Delta z > 0$. Also, due to rotational symmetry, $\vec{R}_{i,i+1}$ is not unique, but for every positive value of $\Delta x(\Delta y)$, the negative equivalent $-\Delta x(-\Delta y)$ can also be used to construct $\vec{R}_{i,i+1}$. This leads to four possible positions for the next neighbor, with four different $\vec{R}_{i,i+1}$ $(\pm\Delta x, \pm\Delta y, \Delta z)$ in a given coordinate system (see Figure 2a). Note that the slip angle θ between the molecular backbone (which also gives the direction of the transition dipole moment) and $\vec{R}_{i,i+1}$ is the same for all four configurations.

We use this consideration to sequentially construct a disordered aggregate chain. The construction starts with the first molecule being placed in the origin of the coordinate system. The second molecule will be placed with respect to the first in one of the four possible positions described above. This assignment is *random*. This procedure extends to all other molecules: the next molecule will always be *randomly* placed with respect to the previously placed adjacent molecule, choosing one of the four possible relative positions. Generally, $\vec{R}_{i,i+1}$ does not have to coincide with $\vec{R}_{i+1,i+2}$, preventing any long-range order and giving rise to *structural* disorder. Since the Δz-value is constant throughout the construction, the aggregate will always "grow" along the z-direction, forming a disordered aggregate chain. Figure 2b shows several possible configurations for the case of a hexamer.

Due to the randomized construction, each aggregate has a different structure. Therefore, a macroscopic object like a thin film must be simulated by an ensemble of different aggregates, each constructed independently of the other.

We next turn to the Hamiltonian that describes the optical properties of the proposed structural model. Each molecule is considered to be a two-level system, corresponding to a ground state $|g\rangle$ and a localized excitation $|i\rangle = b_i^\dagger|g\rangle$, where $b_i^\dagger(b_i)$ is the Pauli operator that creates (annihilates) an exciton on molecule i. The basis considered here is spanned by the one-exciton states $|i\rangle$ and two-exciton states $|i\rangle \otimes |j\rangle$ with $i \neq j$. Two-exciton states are optically dark with respect to transitions from the ground state but become bright for transitions from the one-exciton states, therefore contributing to photoinduced absorption. For the steady-state absorption spectrum, only the one-exciton states are needed, while the transient absorption also probes two-exciton states. In this basis, the Hamiltonian is written as

$$H = \sum_i (E_0 + \Delta E + \delta_i) b_i^\dagger b_i + \sum_{i \neq j} V_{ij} b_i^\dagger b_j \tag{1}$$

commonly known as a Frenkel exciton Hamiltonian.[53,54]

The energy difference between the two molecular levels is denoted as E_0, and its value is obtained from monomer spectra in solution. The exact nature of the electronic transition in nBSQ molecules is associated with the symmetric ground and antisymmetric zwitterionic states but is not required for the present simulation. The solution to the crystal energy shift is denoted by ΔE. The excitation energy of each molecule will be slightly different due to the molecule's local environment. This variation is modeled by including a static disorder δ_i, which is sampled from a Gaussian distribution with a standard deviation σ and zero mean. For simplification, vibronic components in the Hamiltonian are neglected as both its spectral transition strength (Figure 1b) and the associated couplings are small in squaraine dyes.[47,50]

The excitations on different sites are coupled through the resonant coupling V_{ij}. We assume that this interaction is dominated by dipole−dipole interactions and employ the point−dipole approximation

$$V_{ij} = \frac{\mu_i \mu_j}{4\pi\epsilon_0\epsilon_r R_{ij}^3}(1 - 3\cos^2(\theta_{ij})) \tag{2}$$

where μ_i denotes the transition dipole moment (oriented along the molecular backbone) on site i, $R_{ij} = |\vec{r}_i - \vec{r}_j|$ is the distance between the two molecules, and θ_{ij} is the slip angle between the transition dipole moments and the relative position of both molecules, $\vec{R}_{ij}$.

https://doi.org/10.1021/jacs.2c07064
J. Am. Chem. Soc. 2022, 144, 19372−19381

This simple interaction scheme shows the influence of structural disorder, unperturbed by other effects, on the aggregate's optical features. Even in a simple system like a trimer, the structural disorder has a profound influence on the interaction, as portrayed in Figure 2c. The two trimers shown in Figure 2c distinguish two possible alignment cases: *straight* (left) and *kinked* (right). Although both structures feature the same slip angle θ between the nearest neighbors, the next-nearest neighbors' alignment ($\theta_{1,3}$) deviates a lot. While the straight structure always reproduces the same next-nearest angle ($\theta_{1,3} = \theta$), the kinked alignment always changes the angle ($\theta_{1,3} \neq \theta$). This altered angle significantly changes the interaction $V_{1,3}$, potentially even switching it from negative ("J-like") to positive ("H-like"). Moreover, if θ is sufficiently close to the magic angle of 54.7°, the magnitude of the next-nearest neighbor interaction even becomes comparable to the nearest neighbor interaction and influences the optical properties significantly. As "kinks" are more likely, the longer the aggregate gets, the more the non-nearest neighbor interactions become significant. This leads to competing interactions of "J-like" and "H-like" characters, creating a much more complex system than regular J- or H-aggregates.

The absorption spectrum is most easily calculated in the eigenbasis of the Hamiltonian given in eq 1 which is obtained by numerical diagonalization.[53] The absorption spectrum is then calculated as follows

$$A(\epsilon) \propto \left\langle \sum_k \mu_k^2 \epsilon_k f(\epsilon - \epsilon_k, \sigma) \right\rangle \tag{3}$$

where μ_k and ϵ_k are the transition dipole moment and eigenenergy associated with eigenstate k of the Hamiltonian, respectively. The brackets $\langle\ \rangle$ denote the ensemble average over many randomly generated disorder realizations, and $f(\epsilon,\sigma)$ is a Gaussian line shape function centered at $\epsilon = 0$ and with a standard deviation of σ. More information on this calculation can be found in Supporting Information, Part 2.

The transient absorption spectra were calculated considering a sequence of a pump pulse and a probe pulse. The pump pulse can bring an aggregate from its ground state into a one-exciton state. The probe pulse may result in a transition from this one-exciton state into a two-exciton state (excited-state absorption) or in stimulated emission from the one-exciton state back to the ground state. The transient absorption spectrum, being the difference between the probe absorption spectrum and the steady-state absorption spectrum, thus has three contributions: bleaching of the transitions between the ground state and the one-exciton states (negative), stimulated emission of the one-exciton state excited by the pump pulse (negative), and excited-state absorption (positive). A full explanation of the used framework can be found in ref 54 as well as in Supporting Information, Part 2.

To account for dynamical processes, we consider two different exciton occupation populations after photoexcitation by the pump pulse. For short time delays, we estimate the exciton population to reside in the bright state which gets excited by the pump pulse. For longer time delays, we consider a relaxed exciton population which resides in the lowest energy exciton state following a Boltzmann distribution. As the latter exciton occupation does not yield a good fit (see Figure S3), we will from now on only address the exciton population at short time delays unless mentioned differently. Similar to the absorption spectrum, the resulting transient spectra are averaged over a large ensemble of disorder realizations.

COMPUTATIONAL METHODS

The transition dipole moment μ used to evaluate the interaction strength was calculated from the measured attenuation spectrum of monomeric nBSQ, yielding a high value of 15.6 Debye—a reasonable value given the equally high values for gas-phase time-dependent density functional theory calculations (12.6 Debye, see Part 3 of the Supporting Information) as well as essential state model calculations (19.9 Debye). This yields an interaction strength prefactor $\eta = \frac{\mu^2}{4\pi\epsilon_r\epsilon_0}$ of roughly 150 eV Å^3. The transition dipole moment of nBSQ is large in contrast to other molecular dyes, for example, porphyrin (∼6 Debye)[55,56] and perylene (∼8 Debye),[19] which is consistent with the higher extinction coefficient.[49]

The peak of the absorption spectrum of nBSQ in chloroform at 1.91 eV was chosen as the on-site energy E_0. Best fitting spectra were obtained when the static-energy disorder was sampled from a Gaussian distribution with a standard deviation σ of 0.05 eV and a zero mean to account for differences in the monomeric environment inside an aggregate. The stick spectrum was convolved with a narrow Lorentzian line shape with a full width at half maximum (fwhm) of 0.05 eV.

The size of the simulated aggregate ensemble was determined empirically by increasing it to 10^6 aggregates. The resulting density of states and absorbance converged for all aggregate lengths between 3 and 20 molecules if one ensemble contained at least 5×10^4 independently generated aggregates. Hence, 5×10^4 was chosen as the most effective ensemble size. A comprehensive list of all model parameters used in the simulation can be found in Table S1 in Supporting Information, Part 2.

EXPERIMENTAL METHODS

Samples. The nBSQ dye was synthesized and processed to thin films following the previously published procedure,[49] where spin-casted and thermally annealed thin film samples were extensively characterized by spectroscopic ellipsometry and X-ray diffraction. For spectroscopy measurements in solution, nBSQ was dissolved in chloroform, and the solutions were sonicated to ensure complete dissolution. The aggregated thin film was obtained by spin coating onto float glass substrates with a film thickness of ca. 15 nm and thermally annealed at 90 °C under an inert atmosphere to obtain the most stable, fully aggregated sample. Further characterization is provided in the Supporting Information, Part 1.

Steady-State Absorption and Fluorescence Measurements. The static absorption spectra were measured using a Lambda 1050 absorption spectrometer (Perkin & Elmer) at ambient conditions (∼22 °C). For solution sample measurements, an nBSQ stock solution in chloroform was diluted to a concentration of around 1.5×10^{-6} mol l^{-1} and measured in a cuvette with a 5 mm optical path length. Thin film absorption spectra have been corrected for the substrate response.

An LS-55 fluorescence spectrometer (Perkin & Elmer) was used for fluorescence measurements using 620 nm excitation for the monomeric solution and 650 nm for the thin films.

Ultrafast Transient Absorption Spectroscopy. Femtosecond white light spectroscopy was conducted using a spectrometer based on a 125 kHz, Yb:KGW regenerative amplifier laser system (PHAROS, Light Conversion).[57] Band-pass filtered pulses from a non-collinear optical parametric amplifier (NOPA, Light Conversion) were used for pumping the sample with a temporal width of 100−150 fs at 1.72 eV (720 nm). To prevent laser degradation of the aggregated films, the excitation pulse energy was attenuated to around 2 nJ per pulse and slightly focused onto the sample with a spot size of around 200 μm in diameter. For the probe, a 1450 nm laser beam is tightly focused into a 2 mm thick sapphire plate to generate a white light supercontinuum. The white light beam was spectrally filtered, limiting the range to 500−800 nm. The transient spectra were

https://doi.org/10.1021/jacs.2c07064
J. Am. Chem. Soc. 2022, 144, 19372−19381

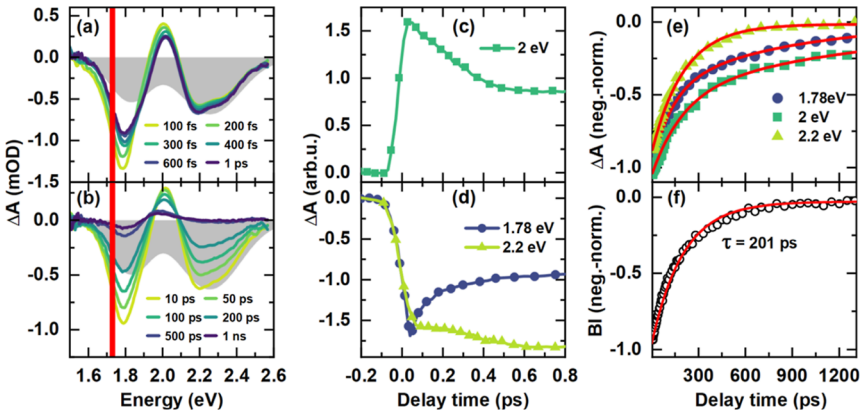

Figure 3. Dispersion-corrected transient absorption spectra at selected delay times and dynamics. The red bar indicates the pump energy. (a) Transient spectra in a short delay time range. (b) Transient spectra in a long delay time range. The gray area indicates the negative absorption profile as a rescaled reference. (c–f) Relaxation dynamics observed at different energies. (c) Short time range at 2.0 eV. (d) Short time range at 1.8 and 2.2 eV. (e) Long time range at 1.78, 2.0 eV (flipped for comparison), and 2.2 eV, renormalized. (f) Band integral dynamics as obtained from eq 3. Dots are experimental data, and red lines are fitted with exponential functions.

detected using a silicon-based diode array mounted in a polychromatic spectrometer (HARPIA, Light Conversion). To minimize pump scattering into the detector, the polarization of the pump beam was set perpendicular to that of the probe, and a polarizer was placed in front of the detector.

RESULTS AND DISCUSSION

Steady-State Absorption. The absorbance of monomeric nBSQ in chloroform solution (gray line in Figure 1b) shows a maximum absorption peak at around 650 nm (1.91 eV), corresponding to the optical HOMO to LUMO transition (S0 → S1).[58,59] The maximum absorption peak has a molar extinction coefficient of around 4×10^5 M^{-1} cm^{-1}.[49] A relatively weak shoulder peak at around 590 nm (2.1 eV) is assigned to the vibronic progression (0–1). The main absorption peak carries a fwhm of around 0.1 eV. In contrast to the monomer, the aggregated thin film exhibits two broad absorption peaks (red line in Figure 1b), one centered at around 1.84 eV (fwhm ≈ 0.25 eV) and another centered at around 2.26 eV (fwhm ≈ 0.4 eV). In contrast to the monomer's absorption spectrum, the higher-energy peak is blue-shifted by around 0.36 eV, while the lower-energy peak is red-shifted by around 0.06 eV. Such a large energy separation between the two peaks must be beyond vibronic coupling. Another intricate aspect is the total quenching of photoluminescence in the aggregated thin film (see Supporting Information Part 4, Figure S1), indicating that the red-shifted peak cannot be ascribed to a regular J-band coinciding with the bottom of the exciton band. Other explanations such as H-aggregation mixing with red-shifted monomers or Davydov-splitting can be safely ruled out as well due to the absence of observable photoluminescence. Our observations are in line with previous reports.[47,49]

Figure 4a shows how the simulated spectrum using the proposed model with structural disorder and dipolar resonant interactions is in agreement with the measured spectrum. The simulation reproduces both the position and the width of both spectral features, where the width is found to be dominated by the structural disorder.

The optimized structural parameters are $N = 10$ molecules, with $\Delta x = 3$ Å, $\Delta y = 1$ Å, and $\Delta z = 3.9$ Å. The latter values deviate from the single-crystal XRD[49]-derived lattice parameters ($\Delta x = 3.52$ Å, $\Delta y = 1.93$ Å, and $\Delta z = 3.34$ Å), suggesting a different structure in thin films and single crystals. The resulting slip angle θ between the molecular axis and the translation vector is 53.3°, which yields a nearest-neighbor interaction energy of −0.08414 eV. Note that the Madelung energy includes both the nearest and non-nearest neighbor interactions and thus will be much bigger. Additionally, the much smaller value for Δy compared to the single crystal results in a slightly bigger slip angle, favoring H-like interactions and increasing the impact of structural disorder.

An important finding of our simulations is that the density of states (gray area) extends below the absorption edge, resulting in low-energy dark states. This is consistent with the observed lack of photoluminescence, as the low-energy dark states are of exciton-band character, providing a fast relaxation channel and therefore following Kasha's rule. While disorder, in general, is predicted to increase the photoluminescence efficiency of H-aggregates,[60] this effect seems not pronounced enough to be visible in our simulation due to the ensemble character of the model, in which most aggregates do have a purely dark lowest energy state. While our model provides an intuitive understanding of the lack of photoluminescence in the thin film sample, other effects might increase the quenching further. The ensemble character of the model provides an efficient platform for reabsorption of emitted photons, which further increases concentration quenching. Forming of other quasiparticles like polarons or excimers as well as adiabatic processes like spin-flips might further enhance this effect, but are outside the scope of this study.

Transient Absorption. To further investigate the origin of the excitonic transitions and their dynamics, we performed transient absorption spectroscopy. In these experiments, the aggregated nBSQ thin film was excited on the low-energy side of the lowest absorption band (1.722 eV/720 nm) and probed by broadband white light (1.5–2.6 eV/500–800 nm). The measured white light dispersion-corrected transient absorption spectra are presented in Figure 3a,b for selected delay times. At earlier delay times, there are four main observations: (1) bleaching of both the lower- and higher-energy peaks appears simultaneously upon excitation, indicating that they stem from the same species and share a common ground state; (2) the amplitude ratio between both peaks differs from the steady-state absorption data; (3) a positive peak appears in the middle of the spectral range at around 2 eV, with a narrower linewidth

https://doi.org/10.1021/jacs.2c07064
J. Am. Chem. Soc. 2022, 144, 19372–19381

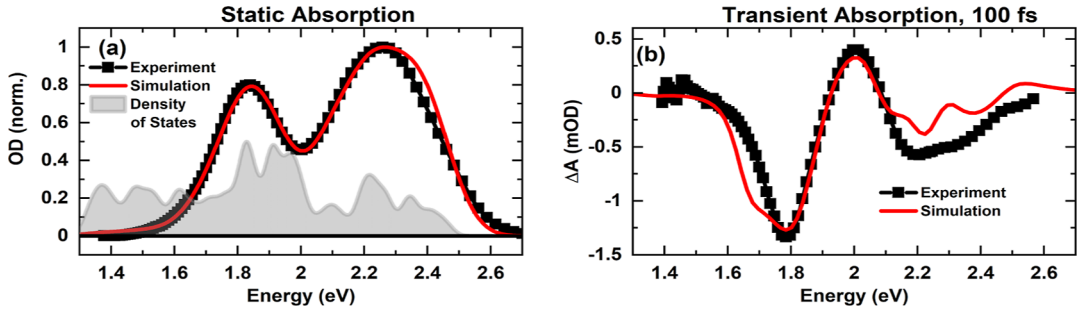

Figure 4. Comparison of the measured and simulated steady-state (a) and transient (b) absorption spectrums of thin film nBSQ. Panel (a) shows the density of states in addition to the absorbance spectrum. Both broad absorption humps are replicated by the simulation, while the density of states below the absorption edge shows the presence of dark states. Panel (b) shows the transient absorption signal at 100 fs after photoexcitation. The decomposition of the transient absorption in terms of ground-state bleach, two-exciton absorption, and stimulated emission is found in the Supporting Information, Part 6, Figure S3.

than the bleach signals; (4) dynamics of the two bleaching signals are different. Similar results were obtained when we exited the aggregated film with a higher energy of 2.43 eV (510 nm) (see Supporting Information Part 5, Figure S2).

Figure 3c−e shows three representative decay curves taken at 1.8, 2.0, and 2.2 eV, respectively, for both short and long delay times. The sub-ps dynamics for the high-energy region is considerably different from the other regions, as the signal is even slowly increasing for the first 800 fs. The non-exponential shape and duration of the growth suggest a more complex mechanism, possibly due to the relaxation of the exciton population into lower-energy states.

Fitted exponential functions (see Figure 3e) indicate that long-time dynamics at 2.2 eV roughly follows a mono-exponential decay with a lifetime of 205 ps, while the other two require at least bi-exponential decay functions. The sub-picosecond rise of the dynamics as well as the nature of the second relaxation channel seen only at long delay times and for a selected energy range cannot intuitively be explained in the context of the exciton-band model of non-interacting aggregate chains and suggests more complex interactions like energy transfer between aggregates, Coulomb screening effects, or charge-transfer interactions.

To gain further insights into the exciton recombination processes, the band integral (BI)[61,62] over the whole observed spectral region at different delay times was calculated from the raw data by using the formula

$$\mathrm{BI}(t) = \int_{1.55\ \mathrm{eV}}^{2.38\ \mathrm{eV}} \frac{\Delta \mathrm{OD}(\epsilon, t)}{\epsilon} \mathrm{d}\epsilon \tag{4}$$

Figure 3f shows the resulting dynamics. The BI dynamics can be fitted by a single-exponential decay with a time constant of 201 ps, similar to the high-energy dynamics. Therefore, the lifetime of excitons in the aggregated nBSQ film is close to 200 ps, which is much longer than in other molecular aggregates[32,63] (usually 10−100 ps) formed by squaraines with relatively flexible molecular structures (with a less pronounced or even no hydrogen bond network); the more rigid molecular backbone of nBSQ may prevent deformation-assisted relaxation pathways.

As the transient response is more complex than just long-lived bleaching of the steady-state absorption at the lower- and higher-energy sides, our simulations must also consider the two-exciton absorption and stimulated emission contributions, as described in the Structural Model and Theory section.

Figure 4b shows the measured and simulated transient absorption spectrum at 100 fs after photoexcitation. A decomposition of the simulated spectrum can be found in Supporting Information, Part 7. The simulated spectrum qualitatively reproduces the main features of the experimental spectrum: (1) simultaneous bleaching of both lower- and higher-energy regions, (2) a higher negative contribution of the low-energy side compared to the higher-energy side, and (3) a positive signal in between.

Deviations between the simulation and experiment can be seen: (i) on the low-energy shoulder of the low-energy hump. Apparently, the measured stimulated emission is much more suppressed than the simulated one. This could be due to reabsorption inside the thin film. (ii) The high-energy signal seems to be too low in the simulation. (iii) The measured data shows a substructure in the transient signal at higher energies, which is also present to an even higher extent in the simulated spectrum. The substructure may be smoothened by including vibrational modes or explicit modeling of a bath, but this is beyond the scope of this paper.

We have not been able to fit longer time transients by a changed occupation distribution as described above. This indicates a more important role of additional, weaker interactions. Examples might be charge-transfer interactions as well as Förster energy transfer between aggregates, which could explain the multitude of relaxation channels seen in the experimental data.

The two-level approximation employed here is mostly valid for disordered one-dimensional chains. It is known, however, that monomer squaraine dyes have a dark second-excited state, which is optically forbidden from the ground state while having a large transition dipole moment from the first excited state.[51] This dark state has much lower energy than the probe pulse (∼1.17 eV). Furthermore, the relative contribution to the transient absorption spectrum resulting from transitions from the superradiant exciton state to the third level of various molecules scales inversely proportional to the aggregate size N.[64] Hence, the effect of these dark states on the results presented here is expected to be small.

Although many different configurations of the slip angle θ and the number of monomers in an aggregate N were simulated here, only the best-fit parameters for θ and N yield a satisfying fit to the steady-state absorption spectra. While θ influences the spectrum by changing the relative strength of the nearest- and non-nearest neighbor interactions, N affects the spectrum in many ways. The aggregate size influences the

https://doi.org/10.1021/jacs.2c07064
J. Am. Chem. Soc. 2022, 144, 19372−19381

width of the signals as well as the relative contribution of high-energy bright states (see Supporting Information, Part 7 and Figure S4a). A possible reason lies in the "edge effect" of a decreasing amount of non-nearest neighbor interactions when approaching the edge of an aggregate chain. Since "H-like" interactions can only occur between the non-nearest neighbors, near the edge, "H-like" interactions become scarce, resulting in more low-energy states. Further understanding of this effect requires a statistical analysis, which is outside the scope of this work.

During our simulation study, we found that the static-energy disorder parametrized by σ and the width of the Lorentzian lineshape Γ only slightly improved the fit. The main broadening of the two humps in the absorption spectrum must therefore be due to the structural disorder in the aggregates (see also Figure S4b). Based on the sensitivity of the simulation to θ and N, which is comparable to aggregate lengths of other molecules,[13,65,66] the best fit results are very robust.

Overall, both the steady-state and initial transient absorption of nBSQ thin films can be explained using the proposed model with only dipolar excitation transfer interactions and structural stacking disorder with reasonable translation distances, not too far away from the lattice parameters found for single crystals. Our data show that structural disorder alone can account for all features of the steady-state absorption spectrum, the lack of photoluminescence of the red-shifted aggregate peak, as well as the large linewidths of both absorption bands. To achieve this, the lattice parameters have been refitted to enhance H-like couplings in the excitonic model. A continuous transient response to photoexcitation over the whole region of absorption underlines that, while there is a multitude of aggregates, both humps originate from the same set of aggregates.

The intrinsic simplicity of the model provides a solid tool for fast simulations of the absorption spectrum and facilitates reverse engineering of structure−property relations. As the computational cost is small compared to more sophisticated techniques, finding fitting parameters for the disordered structure model can be done even on personal computers without the need of clusters or other sources of high computational output. Moreover, we do not need to impose the single-crystal structure onto the thin film, allowing us to find structures which might describe non-crystalline structures better.

The limitations of the proposed model arise from the greatly simplified molecular interaction. The excitonic model considered here can be extended with vibronic coupling, which leads to asymmetric line shapes of the two peaks. Also, intra- and inter-molecular charge-transfer interactions are not included in this study as they were not needed to model the experimental spectra. This is in contrast to the essential states model used in a previous study[47] where charge transfer was included to explain the two-peak absorption spectrum. In this previous study[47] however, a dimer was considered which is not able to generate the competing J- and H-like couplings found in this paper. Including structural disorder in the essential states model may significantly lower the intermolecular charge-transfer coupling required to obtain a two-peak absorption spectrum.

Adding a modest amount of charge transfer could improve the accuracy of our model at long delay times. Considering the long intrinsic lifetime of charges as well as charge-induced spectral distortions could result in a more satisfying agreement between the simulation and experiment.

The degeneracy of the four different alignments considered in our model might also need further tuning considering the alkyl arms of nBSQ. If a C_{2v} symmetry is chosen instead of a D_{2h} symmetry, the alkyl arm would influence the probability of the four possible alignments and potentially even the alignment vector itself. This consideration could broaden the applicability of the structural disorder model to molecules of lower symmetry. In any case, these more advanced aspects of spectral modeling are not necessary to describe the molecular system at hand.

The importance of discussing nBSQ aggregates as disordered is underlined by previous studies,[49] which have shown that nBSQ thin films are isotropic in-plane. Additionally, the intermolecular distances used in this model are similar to single-crystal data,[49] strengthening our claim of a reliable model. A yet pending question is the strong out-of-plane order observed by XRD, as our experimental setup does not allow probing in this direction.

CONCLUSIONS

In conclusion, we have systematically investigated the optical properties of an aggregated thin film of the squaraine derivative nBSQ with a rigid planar molecular structure by using both steady-state and time-resolved spectroscopy methods. The aggregated film showed a complex steady-state absorption spectrum as well as intricate excited-state dynamics. We observed a transient response across the whole absorption spectrum. Through band integration of the transient spectra, we were able to show that the exciton decays with a lifetime of around 200 ps. Using a model with only dipolar excitation transfer interaction and plausible structural (stacking) disorder, we successfully interpreted all observed phenomena in both steady-state and short-time transient absorption spectra, including their exceptionally large linewidth. Our data suggests that disorder alone can qualitatively reproduce all measured optical features. The results and the model analysis presented here can have significant guidance on further control and manipulation of squaraine aggregates for optoelectronic applications.

ASSOCIATED CONTENT

Supporting Information

The Supporting Information is available free of charge at https://pubs.acs.org/doi/10.1021/jacs.2c07064.

Characterization of nBSQ, Hamiltonian model, calculation of simulated spectra, DFT calculations, photoluminescence spectra, transient absorption spectra for high-energy photoexcitation, decomposition of simulated transient absorption spectra, and simulation of static absorption spectra for different aggregate sizes (PDF)

AUTHOR INFORMATION

Corresponding Authors

Robin Bernhardt − *II. Institute of Physics, University of Cologne, D-50937 Cologne, Germany;* orcid.org/0000-0002-0296-8731; Email: bernhardt@ph2.uni-koeln.de

Jingyi Zhu − *II. Institute of Physics, University of Cologne, D-50937 Cologne, Germany; State Key Laboratory of Molecular Reaction Dynamics and Dynamics Research Centre*

for Energy and Environmental Materials, Dalian Institute of Chemical Physics, 116023 Dalian, China; orcid.org/0000-0003-0519-4724; Email: jingyizh@dicp.ac.cn

Paul H. M. van Loosdrecht − *II. Institute of Physics, University of Cologne, D-50937 Cologne, Germany;* orcid.org/0000-0002-3704-9890; Email: pvl@ph2.uni-koeln.de

Authors

Marìck Manrho − *Zernike Insitute for Advanced Materials, University of Groningen, NL-9747 AG Groningen, Netherlands;* orcid.org/0000-0001-5165-8345

Jennifer Zablocki − *Kekulé-Institute for Organic Chemistry and Biochemistry, University of Bonn, D-53121 Bonn, Germany;* orcid.org/0000-0002-2100-4807

Lukas Rieland − *II. Institute of Physics, University of Cologne, D-50937 Cologne, Germany*

Arne Lützen − *Kekulé-Institute for Organic Chemistry and Biochemistry, University of Bonn, D-53121 Bonn, Germany;* orcid.org/0000-0003-4429-0823

Manuela Schiek − *Institute of Physics, University of Oldenburg, D-26129 Oldenburg, Germany; LIOS & ZONA, Johannes Kepler University, A-4040 Linz, Austria; Department of Chemistry, University of Cologne, D-50939 Cologne, Germany;* orcid.org/0000-0002-0108-2998

Klaus Meerholz − *Department of Chemistry, University of Cologne, D-50939 Cologne, Germany*

Thomas L. C. Jansen − *Zernike Insitute for Advanced Materials, University of Groningen, NL-9747 AG Groningen, Netherlands;* orcid.org/0000-0001-6066-6080

Jasper Knoester − *Zernike Insitute for Advanced Materials, University of Groningen, NL-9747 AG Groningen, Netherlands; Faculty of Science, Leiden University, NL-2300 RA Leiden, Netherlands*

Complete contact information is available at: https://pubs.acs.org/10.1021/jacs.2c07064

Author Contributions

The manuscript was written through contributions of all authors. All authors have given approval to the final version of the manuscript.

Notes

The authors declare no competing financial interest.

■ ACKNOWLEDGMENTS

The authors gratefully acknowledge support from the Deutsche Forschungsgemeinschaft (DFG, RTG-2591 "TIDE—Template-designed Organic Electronics"). M.S. thanks the PRO RETINA Foundation as well as the Linz Institute of Technology (LIT-2019-7-INC-313 SEAMBIOF) for funding.

■ REFERENCES

(1) Huang, Y.; Xing, J.; Gong, Q.; Chen, L.-C.; Liu, G.; Yao, C.; Wang, Z.; Zhang, H.-L.; Chen, Z.; Zhang, Q. Reducing Aggregation Caused Quenching Effect through Co-Assembly of PAH Chromophores and Molecular Barriers. *Nat. Commun.* **2019**, *10*, 169.

(2) Manzhos, S.; Chueh, C.-C.; Giorgi, G.; Kubo, T.; Saianand, G.; Lüder, J.; Sonar, P.; Ihara, M. Materials Design and Optimization for Next-Generation Solar Cell and Light-Emitting Technologies. *J. Phys. Chem. Lett.* **2021**, *12*, 4638−4657.

(3) Tan, J.-H.; Chen, W.-C.; Ni, S.-F.; Qiu, Z.; Zhan, Y.; Yang, Z.; Xiong, J.; Cao, C.; Huo, Y.; Lee, C.-S. Aggregation-State Engineering and Emission Switching in D−A−D′ AIEgens Featuring Dual Emission, MCL and White Electroluminescence. *J. Mater. Chem. C* **2020**, *8*, 8061−8068.

(4) Kuehne, A. J. C.; Gather, M. C. Organic Lasers: Recent Developments on Materials, Device Geometries, and Fabrication Techniques. *Chem. Rev.* **2016**, *116*, 12823−12864.

(5) Saikin, S. K.; Eisfeld, A.; Valleau, S.; Aspuru-Guzik, A. Photonics Meets Excitonics: Natural and Artificial Molecular Aggregates. *Nanophotonics* **2013**, *2*, 21−38.

(6) Mei, J.; Leung, N. L. C.; Kwok, R. T. K.; Lam, J. W. Y.; Tang, B. Z. Aggregation-Induced Emission: Together We Shine, United We Soar. *Chem. Rev.* **2015**, *115*, 11718−11940.

(7) Ostroverkhova, O. Organic Optoelectronic Materials: Mechanisms and Applications. *Chem. Rev.* **2016**, *116*, 13279−13412.

(8) Clarke, T. M.; Durrant, J. R. Charge Photogeneration in Organic Solar Cells. *Chem. Rev.* **2010**, *110*, 6736−6767.

(9) Zhang, L.; Cole, J. M. Dye Aggregation in Dye-Sensitized Solar Cells. *J. Mater. Chem. A* **2017**, *5*, 19541−19559.

(10) Xu, F.; Testoff, T. T.; Wang, L.; Zhou, X. Cause, Regulation and Utilization of Dye Aggregation in Dye-Sensitized Solar Cells. *Molecules* **2020**, *25*, 4478.

(11) Kasha, M. Energy Transfer Mechanisms and the Molecular Excitons Model for Molecular Aggregates. *Radiat. Res.* **1963**, *20*, 55−70.

(12) Kasha, M.; Rawls, H. R.; Ashraf El-Bayoumi, M. The Exciton Model in Molecular Spectroscopy. *Pure Appl. Chem.* **1965**, *11*, 371−392.

(13) Würthner, F.; Kaiser, T. E.; Saha-Möller, C. R. J-Aggregates: From Serendipitous Discovery to Supramolecular Engineering of Functional Dye Materials. *Angew. Chem., Int. Ed.* **2011**, *50*, 3376−3410.

(14) Gierschner, J.; Park, S. Y. Luminescent Distyrylbenzenes: Tailoring Molecular Structure and Crystalline Morphology. *J. Mater. Chem. C* **2013**, *1*, 5818−5832.

(15) Spano, F. C.; Silva, C. H- and J-Aggregate Behavior in Polymeric Semiconductors. *Annu. Rev. Phys. Chem.* **2014**, *65*, 477−500.

(16) Kistler, K. A.; Pochas, C. M.; Yamagata, H.; Matsika, S.; Spano, F. C. Absorption, Circular Dichroism, and Photoluminescence in Perylene Diimide Bichromophores: Polarization-Dependent H- and J-Aggregate Behavior. *J. Phys. Chem. B* **2012**, *116*, 77−86.

(17) Zhong, C.; Bialas, D.; Collison, C. J.; Spano, F. C. Davydov Splitting in Squaraine Dimers. *J. Phys. Chem. C* **2019**, *123*, 18734−18745.

(18) Hennessy, M. H.; Pascal, R. A.; Soos, Z. G. Vibronic Structure of Frenkel and Charge-Transfer Excitons in PTCDA. *Mol. Cryst. Liq. Cryst. Sci. Technol., Sect. A* **2001**, *355*, 41−63.

(19) Gisslén, L.; Scholz, R. Crystallochromy of Perylene Pigments: Interference between Frenkel Excitons and Charge-Transfer States. *Phys. Rev. B* **2009**, *80*, 115309.

(20) Eisele, D. M.; Cone, C. W.; Bloemsma, E. A.; Vlaming, S. M.; van der Kwaak, C. G. F.; Silbey, R. J.; Bawendi, M. G.; Knoester, J.; Rabe, J. P.; Vanden Bout, D. A. Utilizing Redox-Chemistry to Elucidate the Nature of Exciton Transitions in Supramolecular Dye Nanotubes. *Nat. Chem.* **2012**, *4*, 655−662.

(21) Didraga, C.; Pugžlys, A.; Hania, P. R.; von Berlepsch, H.; Duppen, K.; Knoester, J. Structure, Spectroscopy, and Microscopic Model of Tubular Carbocyanine Dye Aggregates. *J. Phys. Chem. B* **2004**, *108*, 14976−14985.

(22) Fulton, R. L.; Gouterman, M. Vibronic Coupling. II. Spectra of Dimers. *J. Chem. Phys.* **1964**, *41*, 2280−2286.

(23) Fulton, R. L.; Gouterman, M. Vibronic Coupling. I. Mathematical Treatment for Two Electronic States. *J. Chem. Phys.* **1961**, *35*, 1059−1071.

(24) Yang, M. Influence of Energy Transfer on the Intensity Pattern of Vibronic Excitation Studied by Reduced Density-Matrix Theory. *J. Mol. Spectrosc.* **2006**, *239*, 108−114.

(25) Briggs, J. S.; Herzenberg, A. Sum Rules for the Vibronic Spectra of Helical Polymers. *J. Phys. B: At. Mol. Phys.* **1970**, *3*, 1663−1676.

(26) Briggs, J. S.; Herzenberg, A. Bandshapes in Polymer Spectra. *Mol. Phys.* **1971**, *21*, 865−879.
(27) Eisfeld, A.; Briggs, J. S. The J-Band of Organic Dyes: Lineshape and Coherence Length. *Chem. Phys.* **2002**, *281*, 61−70.
(28) Eisfeld, A.; Briggs, J. S. The J- and H-Bands of Organic Dye Aggregates. *Chem. Phys.* **2006**, *324*, 376−384.
(29) Ajayaghosh, A. Chemistry of Squaraine-Derived Materials: Near-IR Dyes, Low Band Gap Systems, and Cation Sensors. *Acc. Chem. Res.* **2005**, *38*, 449−459.
(30) Liu, T.; Liu, X.; Wang, W.; Luo, Z.; Liu, M.; Zou, S.; Sissa, C.; Painelli, A.; Zhang, Y.; Vengris, M.; Bondar, M. V.; Hagan, D. J.; Van Stryland, E. W.; Fang, Y.; Belfield, K. D. Systematic Molecular Engineering of a Series of Aniline-Based Squaraine Dyes and Their Structure-Related Properties. *J. Phys. Chem. C* **2018**, *122*, 3994−4008.
(31) Law, K. Y.; Chen, C. C. Squaraine Chemistry: Effect of Orientation on the Aggregation of Surfactant Squaraines in Langmuir-Blodgett Films. *J. Phys. Chem.* **1989**, *93*, 2533−2538.
(32) Chen, H.; Farahat, M. S.; Law, K.-Y.; Whitten, D. G. Aggregation of Surfactant Squaraine Dyes in Aqueous Solution and Microheterogeneous Media: Correlation of Aggregation Behavior with Molecular Structure. *J. Am. Chem. Soc.* **1996**, *118*, 2584−2594.
(33) Dimitriev, O. P.; Dimitriyeva, A. P.; Tolmachev, A. I.; Kurdyukov, V. V. Solvent-Induced Organization of Squaraine Dyes in Solution Capillary Layers and Adsorbed Films. *J. Phys. Chem. B* **2005**, *109*, 4561−4567.
(34) Deing, K. C.; Mayerhöffer, U.; Würthner, F.; Meerholz, K. Aggregation-Dependent Photovoltaic Properties of Squaraine/PC61BM Bulk Heterojunctions. *Phys. Chem. Chem. Phys.* **2012**, *14*, 8328−8334.
(35) Chen, G.; Sasabe, H.; Lu, W.; Wang, X.-F.; Kido, J.; Hong, Z.; Yang, Y. J-Aggregation of a Squaraine Dye and Its Application in Organic Photovoltaic Cells. *J. Mater. Chem. C* **2013**, *1*, 6547−6552.
(36) Zhang, Y.; Kim, B.; Yao, S.; Bondar, M. V.; Belfield, K. D. Controlled Aggregation and Enhanced Two-Photon Absorption of a Water-Soluble Squaraine Dye with a Poly(Acrylic Acid) Template. *Langmuir* **2013**, *29*, 11005−11012.
(37) Mayerhöffer, U.; Würthner, F. Cooperative Self-Assembly of Squaraine Dyes. *Chem. Sci.* **2012**, *3*, 1215−1220.
(38) McKerrow, A. J.; Buncel, E.; Kazmaier, P. M. Aggregation of Squaraine Dyes: Structure−Property Relationships and Solvent Effects. *Can. J. Chem.* **1995**, *73*, 1605−1615.
(39) Xu, J.; Zhang, H.; Wang, L.; Liang, G.; Wang, L.; Shen, X.; Xu, W. DFT and TD-DFT Studies on Symmetrical Squaraine Dyes for Nanocrystalline Solar Cells. *Monatsh. Chem.* **2010**, *141*, 549−555.
(40) Wang, X.; Xu, J.; Li, M.; Fang, D.; Chen, B.; Wang, L.; Xu, W. Highly Efficient Unsymmetrical Squaraines for Panchromatic Dye-Sensitized Solar Cells: A Computational Study. *RSC Adv.* **2013**, *3*, 5227−5237.
(41) AL-Fahdan, N. S.; Asiri, A. M.; Irfan, A.; Basaif, S. A.; El-Shishtawy, R. M. An Electro-Optical and Electron Injection Study of Benzothiazole-Based Squaraine Dyes as Efficient Dye-Sensitized Solar Cell Materials: A First Principles Study. *J. Mol. Model.* **2014**, *20*, 2517.
(42) Kaczmarek-Kedziera, A.; Kędziera, D. Molecular Aspects of Squaraine Dyes Aggregation and Its Influence on Spectroscopic Properties. *Theor. Chem. Acc.* **2016**, *135*, 214.
(43) Divya, V. V.; Suresh, C. H. Electronic Structure of Bis(4-Dimethylaminophenyl)Squaraine. *ChemistrySelect* **2019**, *4*, 3387−3394.
(44) Kaczmarek-Kędziera, A.; Żuchowski, P. S.; Kędziera, D. Nature of Intermolecular Interaction in Squaraine Dimers. *Sci. Rep.* **2020**, *10*, 19670.
(45) Balzer, F.; Kollmann, H.; Schulz, M.; Schnakenburg, G.; Lützen, A.; Schmidtmann, M.; Lienau, C.; Silies, M.; Schiek, M. Spotlight on Excitonic Coupling in Polymorphic and Textured Anilino Squaraine Thin Films. *Cryst. Growth Des.* **2017**, *17*, 6455−6466.
(46) Zablocki, J.; Arteaga, O.; Balzer, F.; Hertel, D.; Holstein, J. J.; Clever, G.; Anhäuser, J.; Puttreddy, R.; Rissanen, K.; Meerholz, K.; Lützen, A.; Schiek, M. Polymorphic Chiral Squaraine Crystallites in Textured Thin Films. *Chirality* **2020**, *32*, 619−631.
(47) Hestand, N. J.; Zheng, C.; Penmetcha, A. R.; Cona, B.; Cody, J. A.; Spano, F. C.; Collison, C. J. Confirmation of the Origins of Panchromatic Spectra in Squaraine Thin Films Targeted for Organic Photovoltaic Devices. *J. Phys. Chem. C* **2015**, *119*, 18964−18974.
(48) Zheng, C.; Penmetcha, A. R.; Cona, B.; Spencer, S. D.; Zhu, B.; Heaphy, P.; Cody, J. A.; Collison, C. J. Contribution of Aggregate States and Energetic Disorder to a Squaraine System Targeted for Organic Photovoltaic Devices. *Langmuir* **2015**, *31*, 7717−7726.
(49) Zablocki, J.; Schulz, M.; Schnakenburg, G.; Beverina, L.; Warzanowski, P.; Revelli, A.; Grüninger, M.; Balzer, F.; Meerholz, K.; Lützen, A.; Schiek, M. Structure and Dielectric Properties of Anisotropic N-Alkyl Anilino Squaraine Thin Films. *J. Phys. Chem. C* **2020**, *124*, 22721−22732.
(50) Zheng, C.; Zhong, C.; Collison, C. J.; Spano, F. C. Non-Kasha Behavior in Quadrupolar Dye Aggregates: The Red-Shifted H-Aggregate. *J. Phys. Chem. C* **2019**, *123*, 3203−3215.
(51) Terenziani, F.; Painelli, A.; Katan, C.; Charlot, M.; Blanchard-Desce, M. Charge Instability in Quadrupolar Chromophores: Symmetry Breaking and Solvatochromism. *J. Am. Chem. Soc.* **2006**, *128*, 15742−15755.
(52) D'Avino, G.; Terenziani, F.; Painelli, A. Aggregates of Quadrupolar Dyes: Giant Two-Photon Absorption from Biexciton States. *J. Phys. Chem. B* **2006**, *110*, 25590−25592.
(53) Fidder, H.; Knoester, J.; Wiersma, D. A. Optical Properties of Disordered Molecular Aggregates: A Numerical Study. *J. Chem. Phys.* **1991**, *95*, 7880−7890.
(54) Bakalis, L. D.; Knoester, J. Pump−Probe Spectroscopy and the Exciton Delocalization Length in Molecular Aggregates. *J. Phys. Chem. B* **1999**, *103*, 6620−6628.
(55) Ageeva, T. A.; Bush, A. A.; Golubev, D. V.; Gorshkova, A. S.; Kamentsev, K. E.; Koifman, O. I.; Rumyantseva, V. D.; Sigov, A. S.; Fomichev, V. V. Porphyrin Metal Complexes with a Large Dipole Moment. *J. Organomet. Chem.* **2020**, *922*, 121355.
(56) Oviedo, M. B.; Sánchez, C. G. Transition Dipole Moments of the Qy Band in Photosynthetic Pigments. *J. Phys. Chem. A* **2011**, *115*, 12280−12285.
(57) Jung, E.; Budzinauskas, K.; Öz, S.; Ünlü, F.; Kuhn, H.; Wagner, J.; Grabowski, D.; Klingebiel, B.; Cherasse, M.; Dong, J.; Aversa, P.; Vivo, P.; Kirchartz, T.; Miyasaka, T.; van Loosdrecht, P. H. M.; Perfetti, L.; Mathur, S. Femto- to Microsecond Dynamics of Excited Electrons in a Quadruple Cation Perovskite. *ACS Energy Lett.* **2020**, *5*, 785−792.
(58) Momicchioli, F.; Tatikolov, A. S.; Vanossi, D.; Ponterini, G. Electronic Structure and Photochemistry of Squaraine Dyes: Basic Theoretical Analysis and Direct Detection of the Photoisomer of a Symmetrical Squarylium Cyanine. *Photochem. Photobiol. Sci.* **2004**, *3*, 396−402.
(59) Mayerhöffer, U.; Gsänger, M.; Stolte, M.; Fimmel, B.; Würthner, F. Synthesis and Molecular Properties of Acceptor-Substituted Squaraine Dyes. *Chem.—Eur. J.* **2013**, *19*, 218−232.
(60) Spano, F. C. Modeling Disorder in Polymer Aggregates: The Optical Spectroscopy of Regioregular Poly(3-Hexylthiophene) Thin Films. *J. Chem. Phys.* **2005**, *122*, 234701.
(61) Quick, M.; Kasper, M.-A.; Richter, C.; Mahrwald, R.; Dobryakov, A. L.; Kovalenko, S. A.; Ernsting, N. P. *β*-Carotene Revisited by Transient Absorption and Stimulated Raman Spectroscopy. *ChemPhysChem* **2015**, *16*, 3824−3835.
(62) Sharma, V.; Aharon, S.; Gdor, I.; Yang, C.; Etgar, L.; Ruhman, S. New Insights into Exciton Binding and Relaxation from High Time Resolution Ultrafast Spectroscopy of CH3NH3PbI3 and CH3NH3PbBr3 Films. *J. Mater. Chem. A* **2016**, *4*, 3546−3553.
(63) de Miguel, G.; Ziółek, M.; Zitnan, M.; Organero, J. A.; Pandey, S. S.; Hayase, S.; Douhal, A. Photophysics of H- and J-Aggregates of Indole-Based Squaraines in Solid State. *J. Phys. Chem. C* **2012**, *116*, 9379−9389.

https://doi.org/10.1021/jacs.2c07064
J. Am. Chem. Soc. 2022, 144, 19372−19381

(64) Knoester, J. Nonlinear Optical Susceptibilities of Disordered Aggregates: A Comparison of Schemes to Account for Intermolecular Interactions. *Phys. Rev. A* **1993**, *47*, 2083−2098.
(65) Bakalis, L. D.; Knoester, J. Linear Absorption as a Tool to Measure the Exciton Delocalization Length in Molecular Assemblies. *J. Lumin.* **2000**, *87*−*89*, 66−70.
(66) Arias, D. H.; Stone, K. W.; Vlaming, S. M.; Walker, B. J.; Bawendi, M. G.; Silbey, R. J.; Bulović, V.; Nelson, K. A. Thermally-Limited Exciton Delocalization in Superradiant Molecular Aggregates. *J. Phys. Chem. B* **2013**, *117*, 4553−4559.

https://doi.org/10.1021/jacs.2c07064
J. Am. Chem. Soc. 2022, 144, 19372−19381